Supporting Information

A facile approach to tailor electrocatalytic properties of MnO_2 through tuning phase transition, surface morphology and band structure

Yingze Zhou[a], Zizhen Zhou[a], Long Hu[a], Ruoming Tian[b], Yuan Wang[c], Hamid Arandiyan[c,d], Fandi Chen[a], Mengyao Li[a,*], Tao Wan[a,*], Zhaojun Han[e], Zhipeng Ma[e], Xunyu Lu[e], Claudio Cazorla[f,*], Tom Wu[a], Dewei Chu[a]

[a] *School of Materials Science and Engineering, The University of New South Wales, Sydney 2052, Australia*

[b] *Mark Wainwright Analytical Centre, University of New South Wales, Sydney, NSW 2052, Australia*

[c] *School of Science, RMIT University, Melbourne, Victoria 3001, Australia*

[d] *Laboratory of Advanced Catalysis for Sustainability. School of Chemistry, University of Sydney, Sydney, NSW 2006, Australia*

[e] *School of Chemical Engineering, The University of New South Wales, Sydney 2052, Australia*

[f] *Departament de Física, Universitat Politècnica de Catalunya, Campus Nord B4-B5, E-08034 Barcelona, Spain*

[*] *Corresponding authors.*

E-mail address: mengyao.li1@unsw.edu.au (Mengyao Li)

tao.wan@unsw.edu.au *(Tao Wan)*

claudio.cazorla@upc.edu *(Claudio Cazorla)*

Experimental Section:

Preparation of MnO_2 Nanopowders (the control sample)

α-MnO_2 powder: The α phase MnO_2 powders were synthesized as the control sample to observe the typical morphology of α-MnO_2 using the hydrothermal method.[1] The solution was prepared by dissolving 0.1249 g $KMnO_4$ and 0.0423 g NH_4Cl in 40 mL of deionized water under mechanical stirring. The resulting solution was transferred to a 50-mL Teflon-lined autoclave and then heated at 200 °C for 24 h. After cooling down to room temperature, the MnO_2 products were washed with deionized water and ethanol several times and then dried in air at 80 °C for 12 h.

δ-MnO_2 powder: The δ phase MnO_2 powders were synthesized using a hydrothermal method, which was similar to the reported one.[2] The solution was prepared by dissolving 0.9725 g $KMnO_4$ in 40 mL of deionized water under mechanical stirring. The resulting solution was transferred to a 50-mL Teflon-lined autoclave and then heated at 220 °C for 12 h. After cooling down to room temperature, the MnO_2 products were washed with deionized water and ethanol several times and then dried in air at 80 °C for 12 h.

β-MnO_2 powder: The β phase MnO_2 powders were synthesized using a reported hydrothermal method[3]: 20 ml $KMnO_4$ (0.1 M) and 20 ml $MnSO_4 \cdot H_2O$ (0.6 M) were mixed with continuous stirring for 30 min at room temperature. The mixture solution was transferred to a 50-mL Teflon-lined autoclave and then heated at 140 °C for 12 h. After cooling down to room temperature, the MnO_2 products were washed with deionized water and ethanol several times and then dried in air at 80 °C for 10 h.

Preparation of MnO_2 Electrodes (the control sample)

The working electrode for comparison was prepared by loading sample powders on nickel foam (NF). The NF was cleaned with hydrochloric acid (3.0 M) for 15 min to remove the nickel oxides, followed by rinsing with Milli-Q water and ethanol three times. Then, 5 mg of powders were dispersed into 2.48 mL of DI water and 20 μL of 5 wt% Nafion solution. After that, the mixture solution is put in an ultrasonic bath for 30 min to form a homogeneous ink. Then load 25 μL of catalyst ink on one side of a 0.5 × 2 cm^2 nickel foam (loading size 0.5 × 0.5 cm^2, sample loading mass 0.2 mg cm^{-2}). Finally, the electrode was dried in vacuum at room temperature.

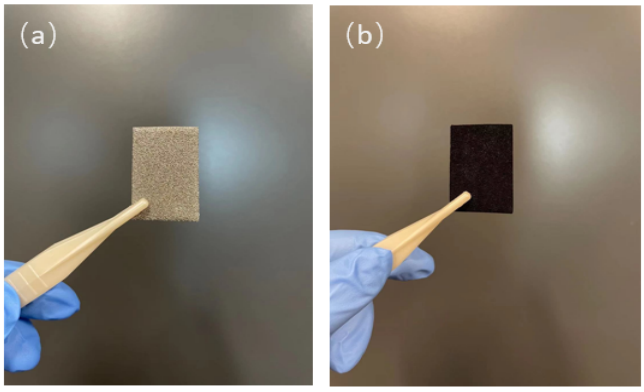

Fig. S1. Photos of NF before and after hydrothermal reaction.

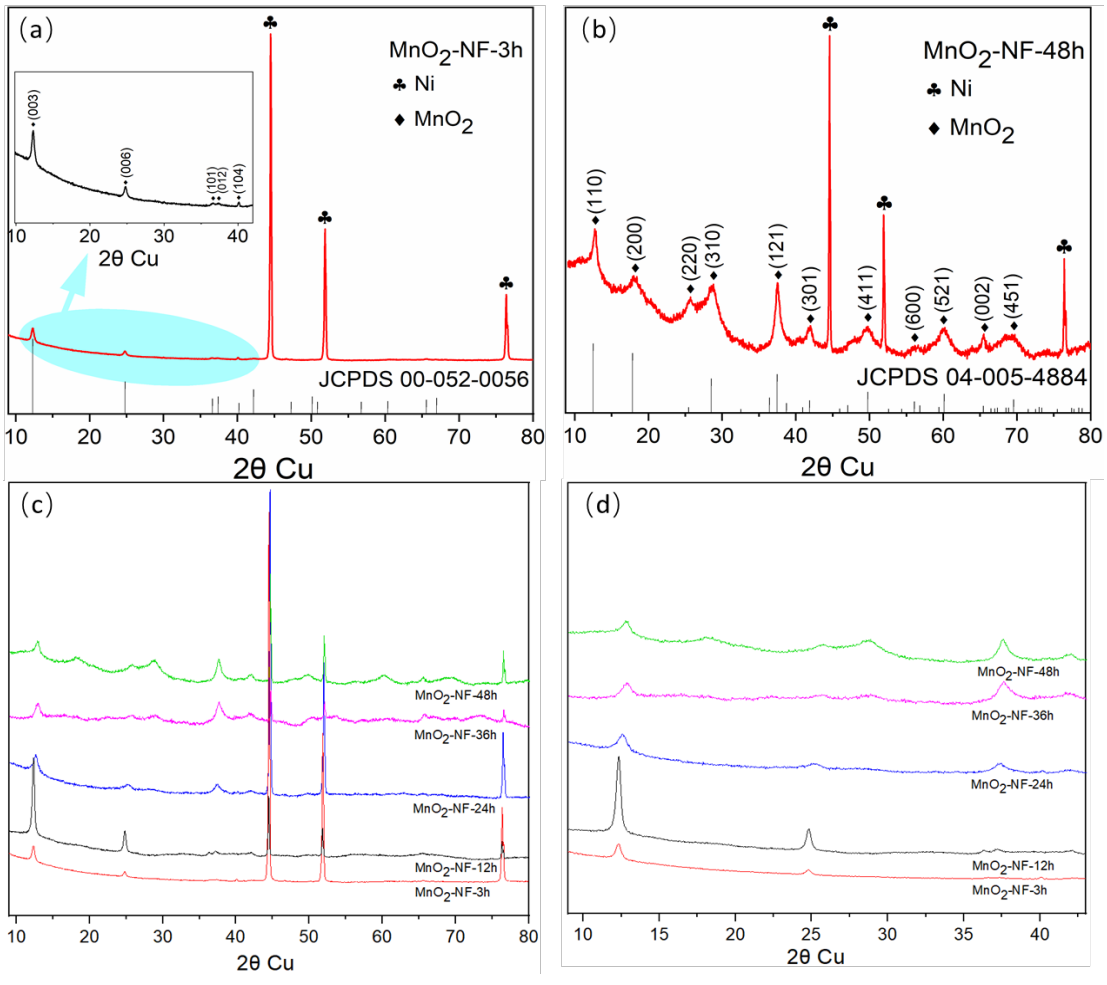

Fig. S2. *(a) XRD patterns of MnO_2-NF-3h; XRD patterns of MnO_2-NF-3h with 2θ from 10 to 40 (inset); (b) XRD patterns of MnO_2-NF-48h;(c) XRD patterns of MnO_2-NF-3h, MnO_2-NF-12h, MnO_2-NF-24h, MnO_2-NF-36h and MnO_2-NF-48h with the 2θ from 9 to 80; (d)XRD*

patterns of MnO_2-NF-3h, MnO_2-NF-12h, MnO_2-NF-24h, MnO_2-NF-36h and MnO_2-NF-48h with the 2θ from 9 to 46.

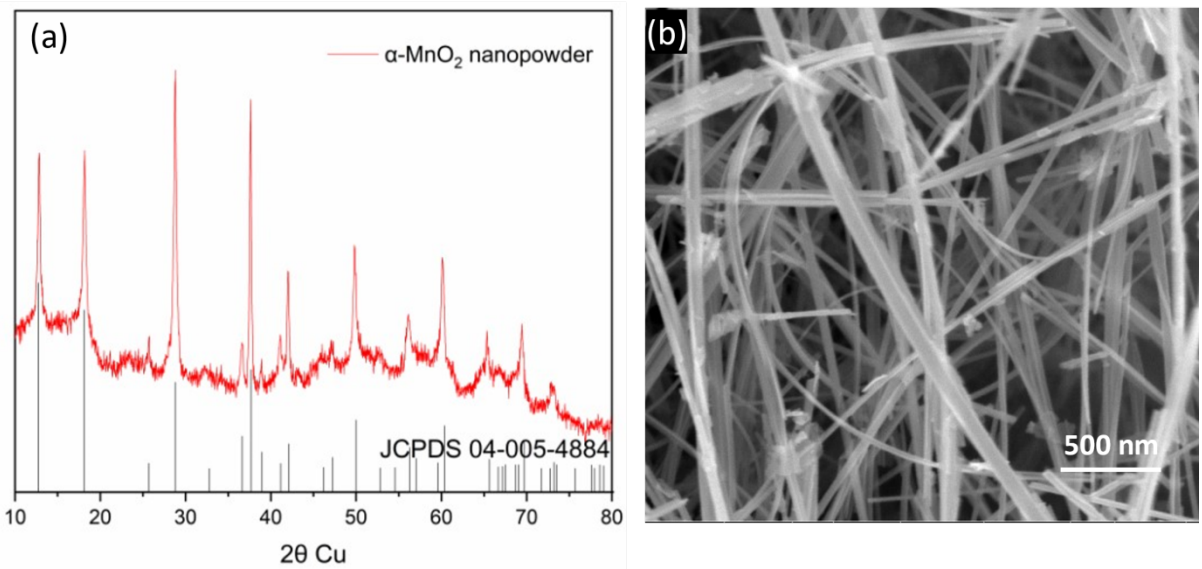

Fig. S3. (a) XRD patterns of alpha MnO_2 nanopowder; (b) Morphologies of alpha phase MnO_2 nanopowder.

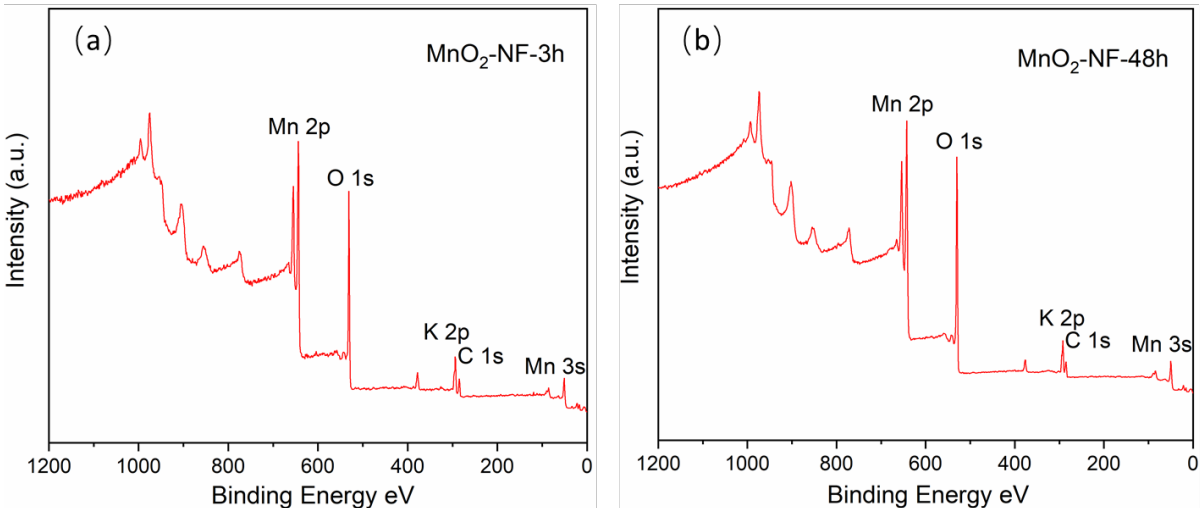

Fig. S4. XPS survey spectrum for (a) MnO_2-NF-3h, and (b) MnO_2-NF-48h.

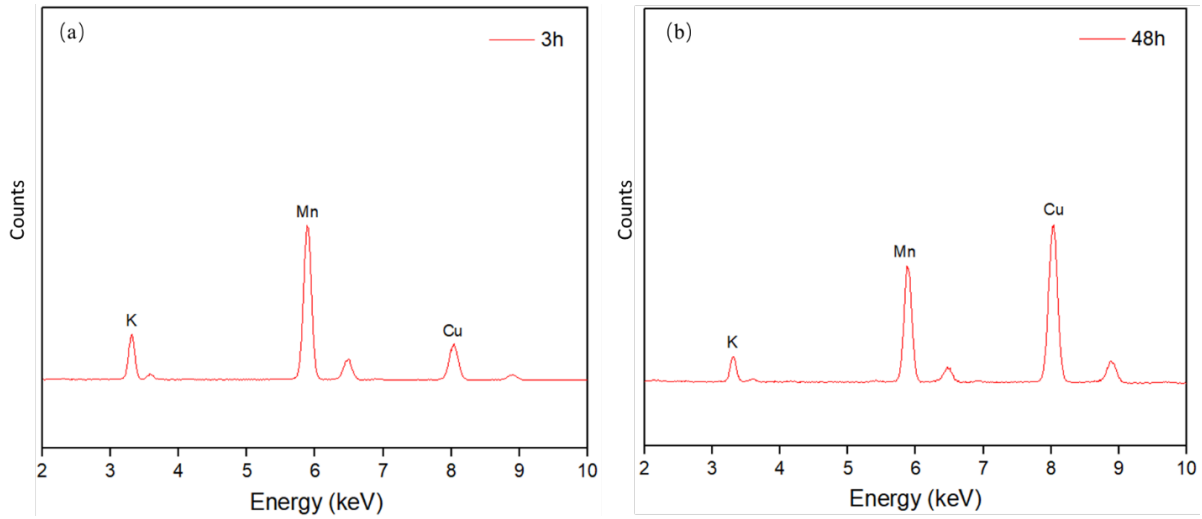

Fig. S5. EDS spectra of element compositional analysis: (a) MnO_2-NF-3h, and (b) MnO_2-NF-48h. The Cu peak is from the TEM copper grid for loading samples.

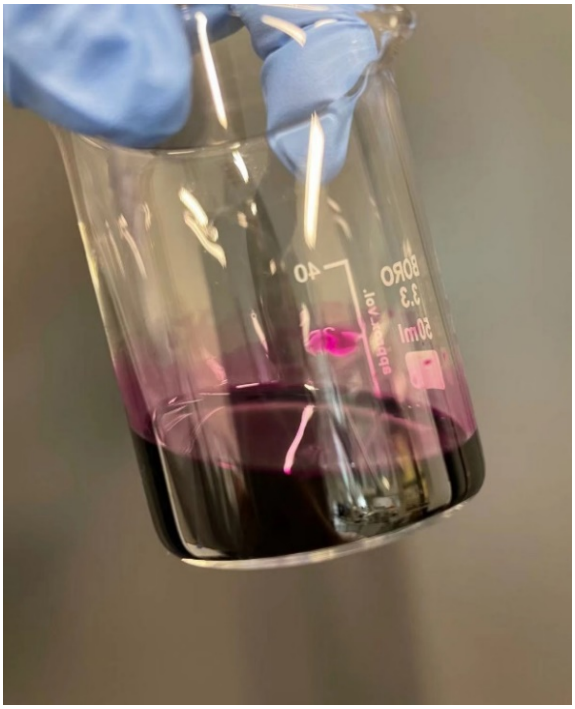

Fig. S6. Photo of solution after 3 hours hydrothermal reaction.

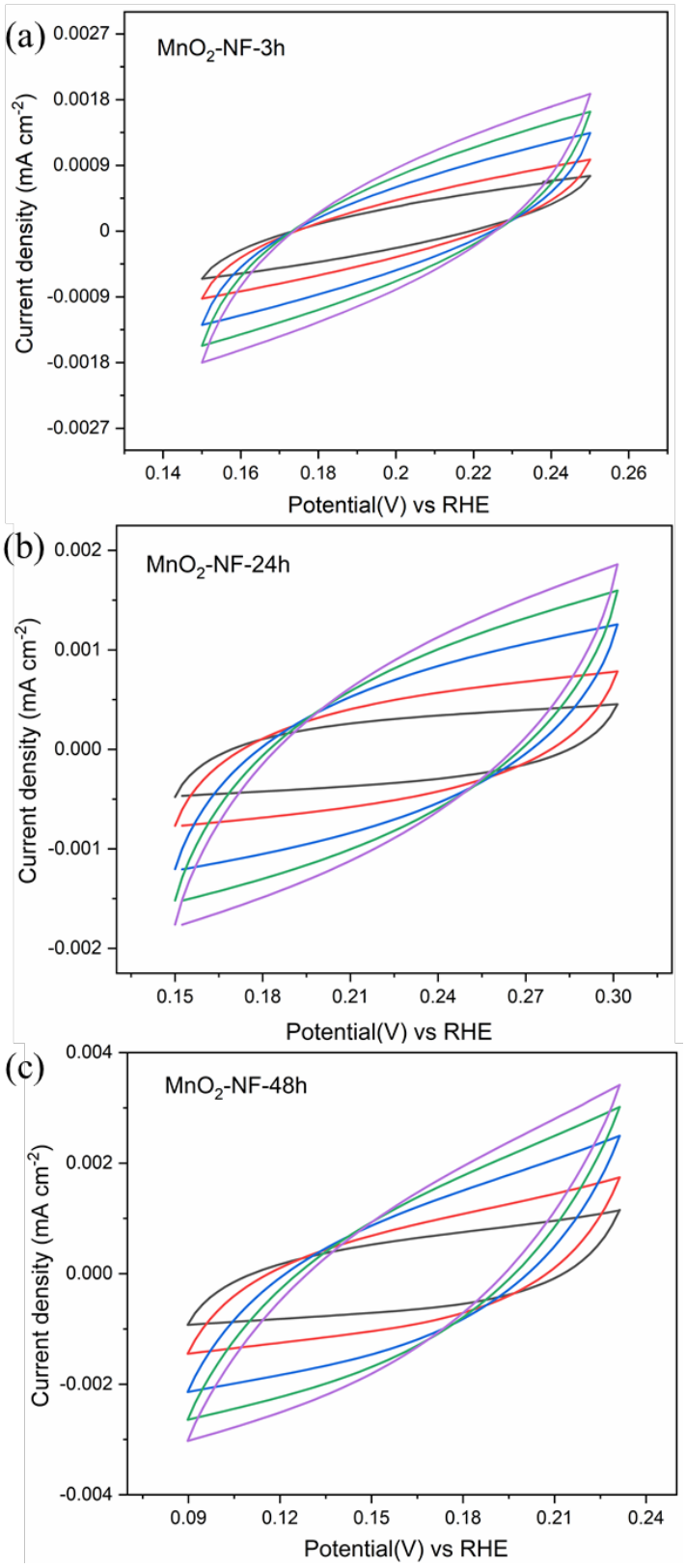

Fig. S7. CVs for (a) MnO_2-NF-3h, (b) MnO_2-NF-24h, and (c) MnO_2-NF-48h measured in a potential window without Faradaic processes at different scan rates: 5, 10, 20, 30, and 40 mV s^{-1}.

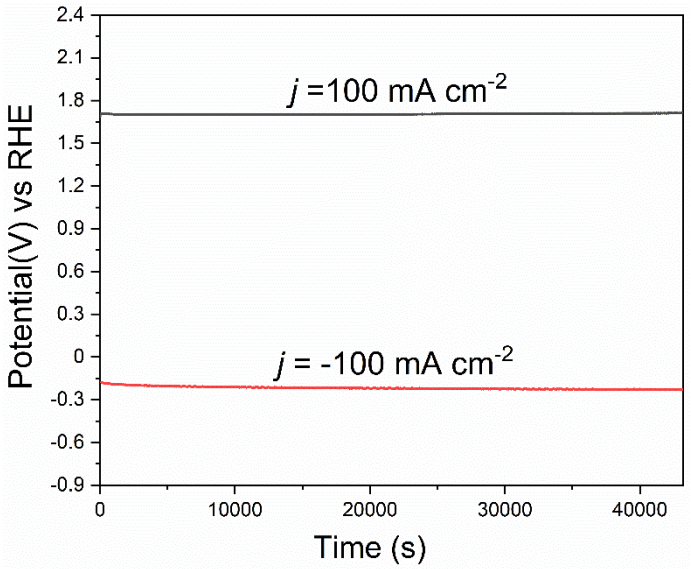

Fig. S8. Chronopotentiometric curve of MnO_2-NF-48h for OER and HER at 100 mA cm^{-2}.

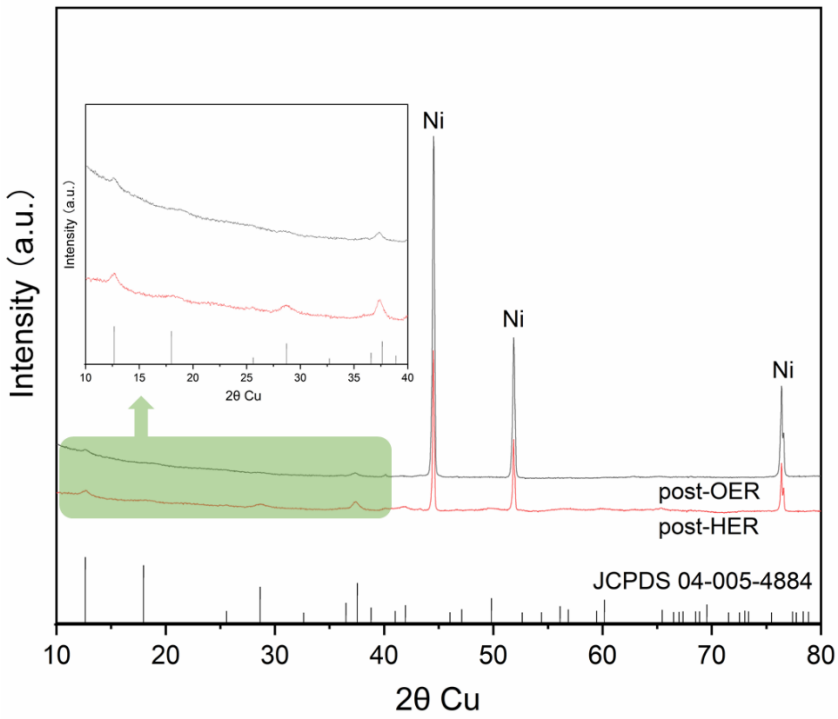

Fig. S9. XRD patterns of post-MnO_2-NF-48h for OER and HER test.

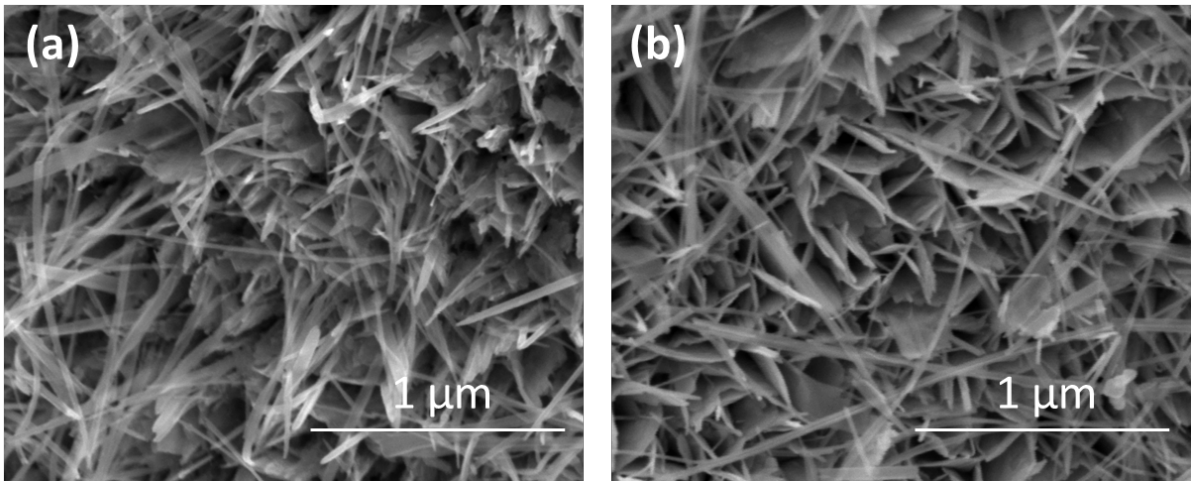

Fig. S10. SEM results of MnO_2-NF-48h after 12 h stability test, (a) OER test, (b) HER test.

Table S1 Comparison with catalytic performances of selected previously reported MnO_2 electrocatalysts.

Catalysts	HER		OER		Electrolyte
	η (V) at j=100 mA cm^{-2}	Tafel slope (mV/dec)	η (V) at j=100 mA cm^{-2}	Tafel slope (mV/dec)	
MnO_2-NF-48h **(This work)**	0.18	110	0.48	123	1 M KOH
NS-MnO_2 [4]	0.35	66	~ 0.44	40	1 M KOH
NF-Ni_3S_2/MnO_2 [5]	0.197	69	~ 0.37	61	1 M KOH
U-CoNi-S-NSA/MnO_2 [6]	~ 0.33	158.2	~ 0.33	73.8	1 M KOH
MnO_2-CoP_3/Ti [7]	/	/	~ 0.37	65	1 M KOH
MnO_2/$NiCo_2O_4$/NF [8]	/	/	~ 0.44	139	1 M KOH
Ni/DMTD/MnO_2 [9]	/	/	> 0.47	/	1 M KOH

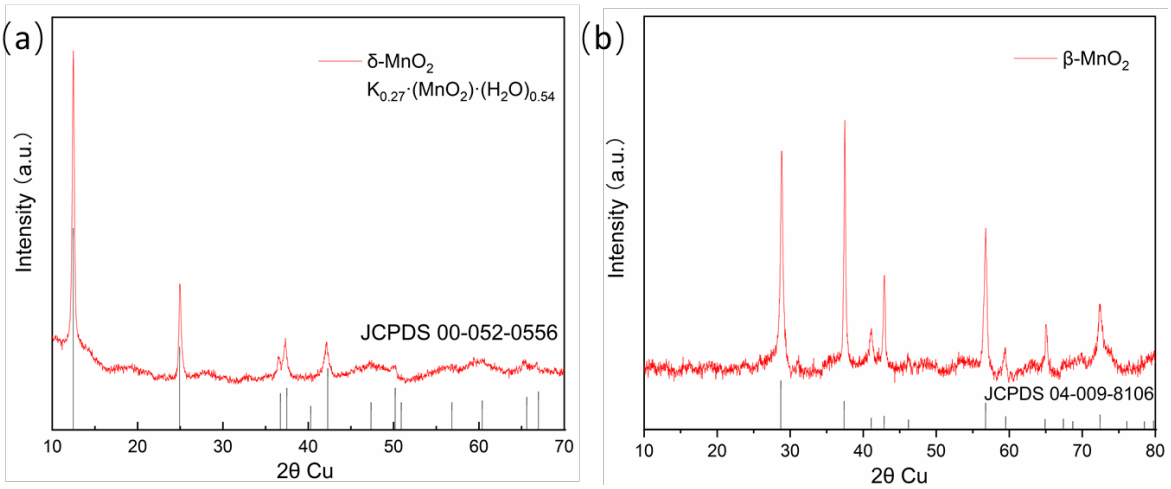

Fig. S11. XRD patterns of δ-MnO_2 and β- MnO_2.

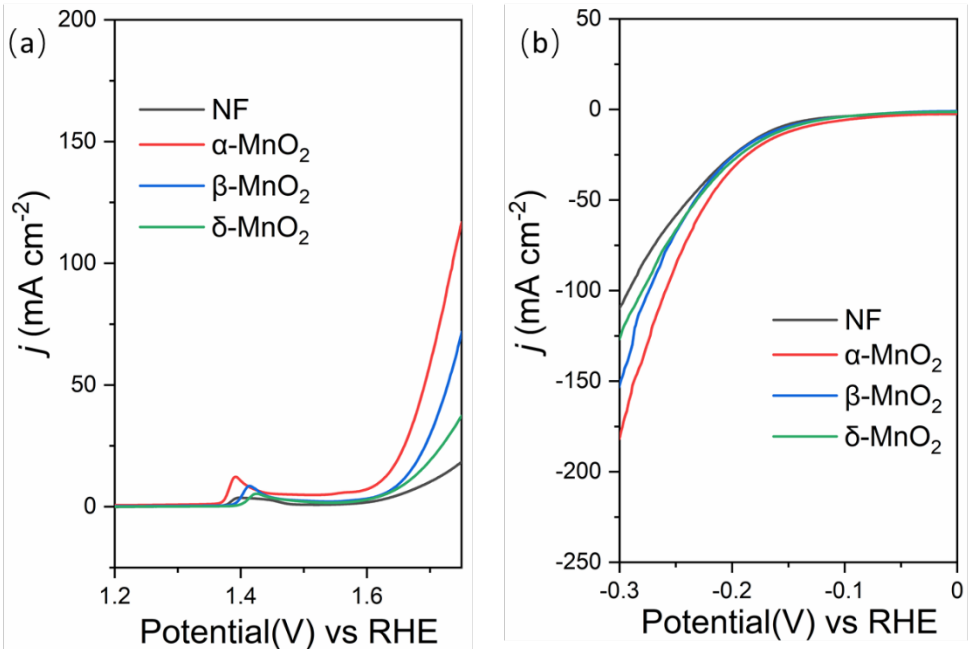

Fig. S12. (a) OER LSV curves of NF, α-MnO_2, δ-MnO_2 and β-MnO_2; (b) HER LSV curves of NF, α-MnO_2, δ-MnO_2 and β-MnO_2.

It is well known that the MnO_2 powder exhibits lower catalytic performance compared to in-situ grown samples.[4] As shown in Fig S12a and b, α-MnO_2 exhibits the best catalytic performance, which is consistent with the previous report.[10] In addition, both α-, β-, and δ-MnO_2 exhibit relatively weak HER performance. The poor contact between active material

and NF, and weak conductivity leads to poor catalytic performance, which proved the advantages of in-situ growth of MnO_2 on NF.

Fig. S13.

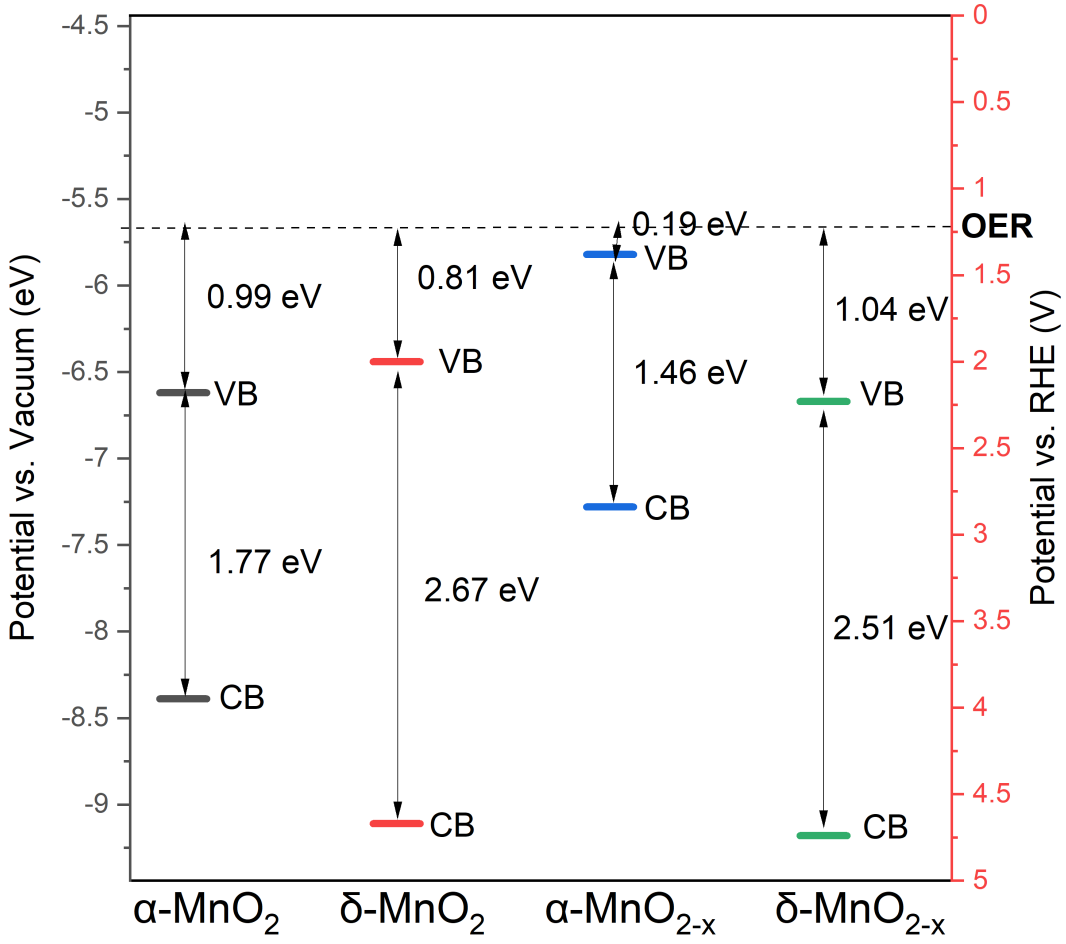

Electronic band structure comparison of α-MnO_2, δ-MnO_2, α-MnO_{2-x} and δ-MnO_{2-x} based on first-principles DFT calculations.

References:

[1] B. Lee, H.R. Seo, H.R. Lee, C.S. Yoon, J.H. Kim, K.Y. Chung, B.W. Cho, S.H. Oh, Critical Role of pH Evolution of Electrolyte in the Reaction Mechanism for Rechargeable Zinc Batteries, ChemSusChem 9 (2016) 2948-2956. https://doi.org/10.1002/cssc.201600702.

[2] X. Li, J. Qu, J. Xu, S. Zhang, X. Wang, X. Wang, S. Dai, K-preintercalated MnO_2 nanosheets as cathode for high-performance Zn-ion batteries, J. Electroanal. Chem. 895 (2021) 115529. https://doi.org/https://doi.org/10.1016/j.jelechem.2021.115529.

[3] N. Zhang, F. Cheng, J. Liu, L. Wang, X. Long, X. Liu, F. Li, J. Chen, Rechargeable aqueous zinc-manganese dioxide batteries with high energy and power densities, Nat. Commun. 8 (2017) 405. https://doi.org/10.1038/s41467-017-00467-x.

[4] Y. Zhao, C. Chang, F. Teng, Y. Zhao, G. Chen, R. Shi, G.I.N. Waterhouse, W. Huang, T. Zhang, Defect-Engineered Ultrathin δ-MnO_2 Nanosheet Arrays as Bifunctional Electrodes for Efficient Overall Water Splitting, Adv. Energy Mater. 7 (2017) 1700005. https://doi.org/10.1002/aenm.201700005.

[5] Y. Xiong, L. Xu, C. Jin, Q. Sun, Interface-engineered atomically thin Ni_3S_2/MnO_2 heterogeneous nanoarrays for efficient overall water splitting in alkaline media, Appl. Catal. B 254 (2019) 329-338. https://doi.org/https://doi.org/10.1016/j.apcatb.2019.05.017.

[6] Q. Hu, X. Liu, B. Zhu, G. Li, L. Fan, X. Chai, Q. Zhang, J. Liu, C. He, Redox route to ultrathin metal sulfides nanosheet arrays-anchored MnO_2 nanoparticles as self-supported electrocatalysts for efficient water splitting, J. Power Sources 398 (2018) 159-166. https://doi.org/https://doi.org/10.1016/j.jpowsour.2018.07.068.

[7] X. Xiong, Y. Ji, M. Xie, C. You, L. Yang, Z. Liu, A.M. Asiri, X. Sun, MnO_2-CoP_3 nanowires array: An efficient electrocatalyst for alkaline oxygen evolution reaction with enhanced activity, Electrochem commun 86 (2018) 161-165. https://doi.org/https://doi.org/10.1016/j.elecom.2017.12.008.

[8] K.-L. Yan, X. Shang, W.-K. Gao, B. Dong, X. Li, J.-Q. Chi, Y.-R. Liu, Y.-M. Chai, C.-G. Liu, Ternary MnO_2/$NiCo_2O_4$/NF with hierarchical structure and synergistic interaction as efficient electrocatalysts for oxygen evolution reaction, J. Alloys Compd. 719 (2017) 314-321. https://doi.org/https://doi.org/10.1016/j.jallcom.2017.05.207.

[9] Y. Han, Y. Yu, L. Zhang, L. Huang, J. Zhai, S. Dong, Facile synthesis of Ni based metal-organic frameworks wrapped MnO_2 nanowires with high performance toward electrochemical oxygen evolution reaction, Talanta 186 (2018) 154-161. https://doi.org/https://doi.org/10.1016/j.talanta.2018.04.026.

[10] Y. Meng, W. Song, H. Huang, Z. Ren, S.-Y. Chen, S.L. Suib, Structure–Property Relationship of Bifunctional MnO_2 Nanostructures: Highly Efficient, Ultra-Stable Electrochemical Water Oxidation and Oxygen Reduction Reaction Catalysts Identified in Alkaline Media, J. Am. Chem. Soc. 136 (2014) 11452-11464. https://doi.org/10.1021/ja505186m.